**CLINICAL STUDY**

# Preferential tumor localization in relation to $^{18}$F-FDOPA uptake for lower-grade gliomas

Hiroyuki Tatekawa[1,2,3] · Hiroyuki Uetani[2] · Akifumi Hagiwara[1,2,4] · Jingwen Yao[1,2,5] · Talia C. Oughourlian[1,2,6] · Issei Ueda[2] · Catalina Raymond[1,2] · Albert Lai[7,8] · Timothy F. Cloughesy[7,8] · Phioanh L. Nghiemphu[7,8] · Linda M. Liau[7,9] · Shadfar Bahri[10] · Whitney B. Pope[2] · Noriko Salamon[2] · Benjamin M. Ellingson[1,2,5,6,7]

## Abstract

**Purpose** Although tumor localization and 3,4-dihydroxy-6-$^{18}$F-fluoro-L-phenylalanine (FDOPA) uptake may have an association, preferential tumor localization in relation to FDOPA uptake is yet to be investigated in lower-grade gliomas (LGGs). This study aimed to identify differences in the frequency of tumor localization between FDOPA hypometabolic and hypermetabolic LGGs using a probabilistic radiographic atlas.

**Methods** Fifty-one patients with newly diagnosed LGG (WHO grade II, 29; III, 22; isocitrate dehydrogenase wild-type, 21; mutant 1p19q non-codeleted,16; mutant codeleted, 14) who underwent FDOPA positron emission tomography (PET) were retrospectively selected. Semiautomated tumor segmentation on FLAIR was performed. Patients with LGGs were separated into two groups (FDOPA hypometabolic and hypermetabolic LGGs) according to the normalized maximum standardized uptake value of FDOPA PET (a threshold of the uptake in the striatum) within the segmented regions. Spatial normalization procedures to build a 3D MRI-based atlas using each segmented region were validated by an analysis of differential involvement statistical mapping.

**Results** Superimposition of regions of interest showed a high number of hypometabolic LGGs localized in the frontal lobe, while a high number of hypermetabolic LGGs was localized in the insula, putamen, and temporal lobe. The statistical mapping revealed that hypometabolic LGGs occurred more frequently in the superior frontal gyrus (close to the supplementary motor area), while hypermetabolic LGGs occurred more frequently in the insula.

**Conclusion** Radiographic atlases revealed preferential frontal lobe localization for FDOPA hypometabolic LGGs, which may be associated with relatively early detection.

✉ Benjamin M. Ellingson
bellingson@mednet.ucla.edu

1 UCLA Brain Tumor Imaging Laboratory (BTIL), Center for Computer Vision and Imaging Biomarkers, David Geffen School of Medicine, University of California Los Angeles, 924 Westwood Blvd., Suite 615, Los Angeles, CA 90024, USA

2 Department of Radiological Science, David Geffen School of Medicine, University of California Los Angeles, Los Angeles, CA, USA

3 Department of Diagnostic and Interventional Radiology, Osaka City University Graduate School of Medicine, Osaka, Japan

4 Department of Radiology, Juntendo University School of Medicine, Tokyo, Japan

5 Department of Bioengineering, Henry Samueli School of Engineering, University of California Los Angeles, Los Angeles, CA, USA

6 Neuroscience Interdepartmental Program, David Geffen School of Medicine, University of California Los Angeles, Los Angeles, CA, USA

7 UCLA Neuro-Oncology Program, David Geffen School of Medicine, University of California Los Angeles, Los Angeles, CA, USA

8 Department of Neurology, David Geffen School of Medicine, University of California Los Angeles, Los Angeles, CA, USA

9 Department of Neurosurgery, David Geffen School of Medicine, University of California Los Angeles, Los Angeles, CA, USA

10 Department of Molecular and Medical Pharmacology, David Geffen School of Medicine, University of California, Los Angeles, CA, USA

## Introduction

Tumor localization is a key factor in the care of patients with lower-grade glioma (LGG) as it correlates with their demographic characteristics, molecular status, clinical presentation, surgical management, and survival time. For example, LGGs were more likely to invade the insula in elderly patients than in young patients, where they tended to localize in the temporal lobe [1]. From a molecular standpoint, only 20% of isocitrate dehydrogenase (IDH) wild-type gliomas were localized in the frontal lobe, while IDH mutant LGGs, especially with 1p19q co-deletion, were more likely to occur in the frontal lobe [2–4]. LGGs in the frontal lobe were associated with a higher risk of preoperative seizure episodes [5]. With regards to surgical intervention, LGGs involved in the insular region were associated with decreased extent of resection and unfavorable prognosis, while patients with the frontal lobe LGGs experienced more thorough resection and exhibited more favorable prognosis than patients with LGGs in the other lobes [6]. For the evaluation of tumor distribution, several studies employed a probabilistic magnetic resonance imaging (MRI)-based brain atlas to specify the probability of anatomical tumor localization associated with the patients' characteristics (age and sex) [7], clinical presentation (symptoms and Karnofsky performance) [8], and molecular status (IDH, epidermal growth factor receptor, O6-methylguanine methyltransferase, and phosphatase and tensin homolog) [9, 10].

Amino acid positron emission tomography (PET), including 3,4-dihydroxy-6-^{18}F-fluoro-L-phenylalanine (FDOPA) and O-2-^{18}F-fluoroethyl-L-tyrosine (FET), is often used as a clinical tool in neuro-oncology to identify metabolically active tumor tissue. FDOPA PET was reported to be superior to FET PET for visualization of primary and recurrent LGGs for lesions outside the striatum, while FET PET benefits from the lower striatal uptake, especially in cases with tumor localization in the basal ganglia [11]. Using either tracer, higher amino acid tracer uptake was associated with higher tumor grade and shorter overall or progression-free survival [12–14]. Molecular status, including IDH mutation and 1p19q codeletion, may also have an association with amino acid tracer uptake, although they are still debated [15–20].

Tumor localization and FDOPA uptake may have an association with each other and cooperatively influence the prognosis of patients with LGGs; however, preferential tumor localization in correlation with varying FDOPA uptake has not yet been investigated. The purpose of this study was to identify differences in frequency of localization between FDOPA hypometabolic and hypermetabolic LGGs using a probabilistic MRI-based brain atlas, and to evaluate overall survival (OS) with different FDOPA metabolic status. We hypothesized that delineation of spatial patterns of preferential tumor localization in relation to FDOPA uptake may improve understanding of underlying tumor pathophysiology and may also lead to appropriate subsequent management.

## Materials and methods

### Patient selection

A total of 51 adult patients (age > 20 years) with newly diagnosed and histologically confirmed LGGs (World Health Organization [WHO] grade II or III) who underwent FDOPA PET and MRI between 2007 and 2019 were retrospectively selected. All patients were diagnosed with LGGs according to the WHO 2007 or 2016 classification, and were classified based on IDH mutational status and 1p19q codeletion status by conventional techniques [21]. No patients underwent stereotactic biopsy prior to FDOPA PET or MRI. OS was measured from the time of the PET scan until death or the censored date (maximum, 2000 days) with median term of 740 days. All patients signed institutional review board-approved consent forms to have their imaging, clinical, and molecular data included in our research database (IRB IRB#10-000655). The patient cohort in this study was partly overlapped with previous studies [22, 23].

### FDOPA PET image acquisition

FDOPA PET images were acquired with a full-ring PET/CT scanner (ECAT-HR; CTI/MIMVista; Siemens, Knoxville, TN, USA) after the subjects fasted for more than four hours. Following previously reported procedures, FDOPA was synthesized and injected intravenously [24, 25]. Computed tomography images were acquired prior to the PET scan for attenuation correction. Three-dimensional FDOPA emission data were acquired for a total of 30 min, and the data were integrated between 10 and 30 min following the injection to obtain 20-min static FDOPA images after reconstruction. FDOPA PET images were then reconstructed using an ordered-subset expectation maximization iterative reconstruction algorithm (six iterations with eight subsets) [26, 27]. Finally, a Gaussian filter with a full width at half maximum of 4 mm was applied. The resulting voxel sizes were 1.34 mm × 1.34 mm × 3 mm for FDOPA PET images. Standardized uptake value (SUV) maps of FDOPA were calculated based on the radioactive activity divided by the decay-corrected injected dose per body mass [28],

and resulting SUV maps were subsequently normalized relative to the median value of the normal-appearing striatum (nSUV) [21, 29].

## Magnetic resonance image acquisition

Anatomical MRI consisted of standard T1-weighted pre- and post-contrast images (2D axial turbo spin echo with 3-mm slice thickness with no interslice gap, or 3D inversion-prepared gradient echo images with isotropic 1–1.5 mm slice thickness) and T2-weighted fluid-attenuated inversion recovery (FLAIR) images acquired at 3-mm slice thickness with no interslice gap using a 1.5-T or 3-T clinical MRI scanner.

## Postprocessing and ROI analysis

The processing procedures are described in Fig. 1. A single tumor region of interest (ROI) was segmented based on the regions of hyperintensity on T2-weighted FLAIR images by a board-certified neuroradiologist (H.T. with 12 years of clinical experience) with Analysis of Functional NeuroImages software (AFNI; NIMH Scientific and Statistical Computing Core; Bethesda, MD, USA; https://afni.nimh.nih.gov) using a semi-automatic procedure as previously described

[30, 31]. FLAIR and PET images, as well as FLAIR hyperintense ROIs were registered to the post-contrast T1-weighted images for each patient using a six-degree of freedom rigid transformation and a mutual information cost function using FSL software (*flirt*; FMRIB, Oxford, UK; http://www.fmrib.ox.ac.uk/fsl/). Each registered ROI was applied to the corresponding PET images. Maximum nSUV ($nSUV_{max}$) within the FLAIR hyperintense ROI and biological tumor volume (BTV), which included the voxels within the ROI higher than the median uptake value in the striatum, were calculated. The LGG patients were stratified into FDOPA hypometabolic ($nSUV_{max} < 1$) and hypermetabolic ($nSUV_{max} > 1$) groups according to the $nSUV_{max}$ with a cut-off value of one relative to the striatum. This cut-off value, one, is determined according to the previous suggestion [32]. Anatomical FLAIR volume and BTV are reported as milliliters.

Each post-contrast T1-weighted images was registered to a 1.0 mm isotropic T1-weighted brain atlas (MNI152; Montreal Neurological Institute [MNI]) using a 12-degree of freedom affine transformation with statistical parametric mapping 12 software (SPM12; Wellcome Trust Centre for Neuroimaging, London, UK; https://www.fil.ion.ucl.ac.uk/spm/software/spm12/), and applied the transform matrix to each FLAIR ROI. The registered ROIs in the left hemisphere
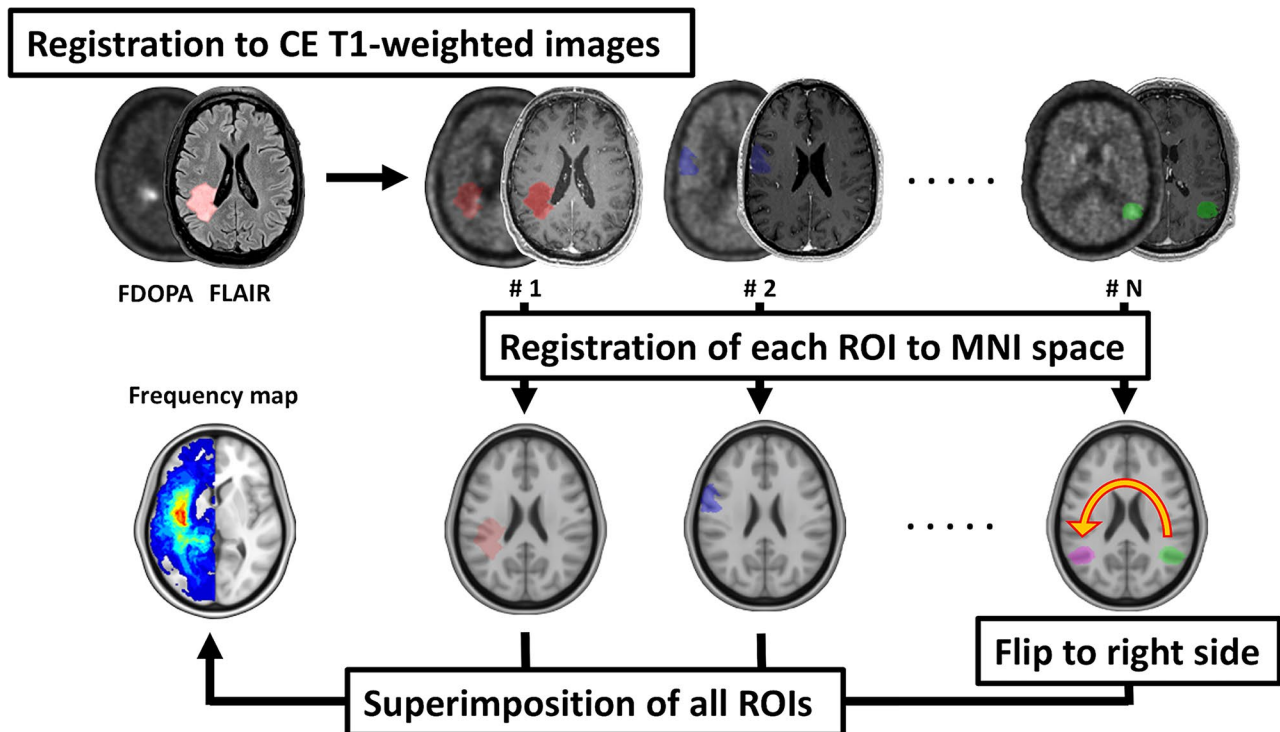


**Fig. 1** Overview of post-processing of MR and PET images. FLAIR and FDOPA images, as well as FLAIR hyperintense ROIs, are registered to the post-contrast T1-weighted images for each patient. Each registered ROI is applied to the corresponding PET images, and maximum nSUV and biological tumor volume within the ROI are calculated. Each registered ROI is then registered to a T1-weighted brain atlas (MNI152) using SPM12. The registered ROI in the left hemisphere is flipped to the right hemisphere in the MNI space. All ROIs in the MNI space are superimposed to create a voxel-wise frequency map for each group

were flipped to the right hemisphere in the MNI space. All tumor ROIs in the MNI space were superimposed to create a voxel-wise frequency map of tumor occurrence in the hypometabolic and hypermetabolic groups separately, and used for the following analysis of differential involvement (ADIFFI) statistical mapping technique [9, 10].

## Statistical analyses

The demographic (sex, age, WHO grade), molecular (IDH/1p19q) status, initial symptoms (seizure; focal neurological deficit, i.e. aphasia, hemiparesis, and muscle weakness; neurological symptoms, i.e. optic/olfactory/hearing/tasting abnormalities, dizziness, and vertigo; headache; other symptoms, i.e. mental/personality changes, unusual feelings; or incidental), and imaging metrics ($nSUV_{max}$ and FLAIR volume) were compared between the FDOPA hypometabolic and hypermetabolic LGGs using the Fisher's exact or Mann–Whitney U test.

ADIFFI consisted of first constructing a $2 \times 2$ contingency table comparing two differential phenotypes (e.g. phenotypes A and B) and tumor versus non-tumor for each image voxel. Next, a two-tailed Fisher's exact test was performed on a voxel-wise basis. According to the Fisher's exact test, the probability of obtaining an observed pattern in the $2 \times 2$ contingency table is given by

$$p = \frac{(a+b)!(c+d)!(a+c)!(b+d)!}{a!b!c!d!n!},$$

where $a$ is the frequency of tumor occurrence in a particular voxel for phenotype A; $b$ the frequency of tumor occurrence in a particular voxel for phenotype B; $c$ the frequency of no tumor occurring in a particular voxel for phenotype A; $d$ the frequency of no tumor occurring in a particular voxel for phenotype B; $n$ the total number of patients; and the exclamation point represents the factorial operation. To calculate the significance of the observed pattern, the contingency table corresponded to the total probability of observing a pattern in the contingency table as extreme or more extreme. Then, the $p$ value was recalculated from each voxel for all cases in which the marginal totals were the same as the observed tables, and only for cases in which the arrangement was as extreme as the observed pattern. We performed this iteratively so that values were incremented to calculate a more extreme pattern, adding the previous $p$ value in each image voxel each time until the most extreme pattern was achieved, which varied from voxel to voxel. The final $p$ value represents the probability of observing the given pattern in the contingency table by chance. The $p$ values less than 0.05 were considered significant. Additional details are presented in a previous publication [9].

For the cluster-based permutation correction outlined by Bullmore et al. [33] a total of 500 random permutations were performed, the resulting ADIFFI-defined clusters with a connection of 18 directions were retained, and the 95% confidence interval (CI) for significant cluster size occurring by chance were documented. The cluster-size thresholds had a 5% probability of occurring by chance.

ADIFFI and cluster-based correction were additionally performed between different age, FLARI volume, or BTV with cut-off of the median value, and also among different molecular statuses.

Kaplan–Meier curves were used to depict differences in the OS, and the log-rank test was employed to compare OS between the FDOPA hypometabolic and hypermetabolic LGGs. Cox univariate regression analyses were conducted to investigate the association of OS with the age, $nSUV_{max}$, and FLAIR volume, and BTV.

Statistical analyses were performed using MATLAB (R2019b; MathWorks, Natick, MA, USA) and GraphPad Prism (Version 8.3; GraphPad Software, La Jolla, CA, USA).

## Results

Table 1 summarizes patient demographics and molecular information, while Supplemental Table 1 describes each patient in more detail. The current study included 51 newly diagnosed patients with gliomas with a median age of 52 years at the time of the PET examination. The patient cohort consisted of 31 males and 20 females. According to 2007 or 2016 WHO criteria, 29 patients had grade II, and 22 had grade III gliomas. A total of 21 gliomas were IDH wild-type, 16 were IDH mutant 1p19q non-codeleted, and 14 were IDH mutant 1p19q codeleted. When comparing between different FDOPA metabolic status, patients with FDOPA hypometabolic LGGs (n = 14, $nSUV_{max}$ < 1) were significantly younger than patients with hypermetabolic LGGs (n = 37, $nSUV_{max}$ > 1) ($p = 0.014$). There were no significant differences between FDOPA hypometabolic and hypermetabolic LGGs in the ratio of the WHO grade ($p = 0.54$), IDH/1p19q mutation status ($p = 0.57$), nor initial symptoms ($p = 0.43$). The volumes of the FLAIR ROIs were significantly smaller in FDOPA hypometabolic than hypermetabolic LGGs ($p = 0.012$).

Figure 2 shows a voxel-wise frequency map calculated by superimposition of tumor ROIs on the MNI brain template for FDOPA hypometabolic and hypermetabolic LGGs. In both groups, tumors mainly localized at the frontal lobe, temporal lobe, insula, and putamen. For FDOPA hypometabolic LGGs, a high number of lesions localized in the frontal lobe. For FDOPA hypermetabolic LGGs, a high number of lesions localized in the insula, putamen, and temporal lobe.

**Table 1** Patient demographics and imaging metrics

|  | Total | FDOPA hypometabolic LGGs | FDOPA hypermetabolic LGGs | $p$ value |
|---|---|---|---|---|
| Number of patients | 51 | 14 | 37 | |
| Female (%) | 20 (39) | 8 (57) | 12 (32) | .12[a] |
| Age (median [IQR], year) | 52 (37, 61) | 47 (27, 51) | 57 (39, 63) | .014[b]* |
| WHO classification grade | | | | .54[a] |
| II (%) | 29 (57) | 9 (64) | 20 (54) | |
| III (%) | 22 (43) | 5 (36) | 17 (46) | |
| IDH mutation and 1p19q codeletion status | | | | .57[a] |
| Wild-type (%) | 21 (41) | 5 (36) | 16 (43) | |
| Mutant 1p19q non-codeleted (%) | 16 (31) | 6 (43) | 10 (27) | |
| Mutant 1p19q codeleted (%) | 14 (27) | 3 (21) | 11 (30) | |
| Initial symptom | | | | .43[a] |
| Seizure (%) | 13 (25) | 3 (21) | 10 (27) | |
| Focal neurological deficit (%) | 6 (12) | 1 (7) | 5 (14) | |
| Neurological symptoms (%) | 10 (20) | 3 (21) | 7 (19) | |
| Headache (%) | 6 (12) | 0 (0) | 6 (16) | |
| Other symptoms (%) | 8 (16) | 3 (21) | 5 (14) | |
| Incidental (%) | 8 (16) | 4 (28) | 4 (11) | |
| $nSUV_{max}$ (median [IQR]) | 1.16 (0.97, 1.48) | 0.94 (0.86, 0.96) | 1.28 (1.13, 1.64) | < .001[b]* |
| Volume of FLAIR hyperintense regions (median, IQR, mL) | 29.7 (13.2, 63.9) | 12.3 (6.0, 31.5) | 44.0 (18.2, 82.5) | .012[b]* |

*LGG* lower grade glioma, *IQR* interquartile range, *IDH* isocitrate dehydrogenase, $nSUV_{max}$ maximum normalized standard uptake value

*Means statistically significant

[a]Uses Fisher's exact test

[b]Uses Mann–Whitney U test

ADIFFI statistical analysis of LGGs based on the FDOPA metabolic status identified two spatially distinct clusters which showed a statistical significance (Fig. 3). One was localized in the frontal lobe, especially in the superior frontal gyrus, while the other was localized in the insula to putamen. The cluster localized in the superior frontal gyrus was associated with more frequent occurrence of FDOPA hypometabolic LGGs. The cluster localized in the insula to putamen was associated with more frequent occurrence of FDOPA hypermetabolic LGGs.

The preferential tumor localization in different age, FLAIR volume, BTV, or molecular status are shown in Supplemental Fig. 1–6. In brief, LGGs in younger patients (age < 52 years) preferentially localized in the frontal lobe (especially in the superior frontal gyrus and pars orbitalis to pars triangularis) and in the temporal lobe (especially in the fusiform gyrus). LGGs in older patients (age ≥ 52 years) did not have preferential localization. LGGs with smaller FLAIR volume (< 29 mL) or BTV (< 0.22 mL) did not show preferential localization. There was no preferential localization between either pair of different IDH/1p19q molecular status.

The Kaplan–Meier curves and log-rank tests showed a significant difference in OS between FDOPA hypometabolic and hypermetabolic LGGs (Fig. 4, $p = 0.046$), with longer survival in FDOPA hypometabolic LGGs. The Cox univariate analysis demonstrated a significant increase in hazard associated with the patient's age (hazard ratio [HR] 1.075, 95% CI [1.003, 1.152], $p = 0.042$), but not with the $nSUV_{max}$ (HR 1.403, 95% CI [0.670, 2.937], $p = 0.37$), FLAIR volume (HR 0.997, 95% CI [0.977, 1.017], $p = 0.74$), or BTV (HR 1.056, 95% CI [0.991, 1.125], $p = 0.089$).

## Discussion

In the current study, frequency of localization for gliomas with different FDOPA metabolic status was evaluated using a probabilistic MRI-based brain atlas. The FDOPA hypometabolic LGGs occurred more frequently in the frontal lobe, especially in the superior frontal gyrus, while the FDOPA hypermetabolic LGGs occurred more frequently in the insula. The log-rank test identified significantly longer survival in FDOPA hypometabolic LGGs compared with hypermetabolic LGGs.

The frontal lobe, especially the supplementary motor area (SMA), and the insular area have previously been
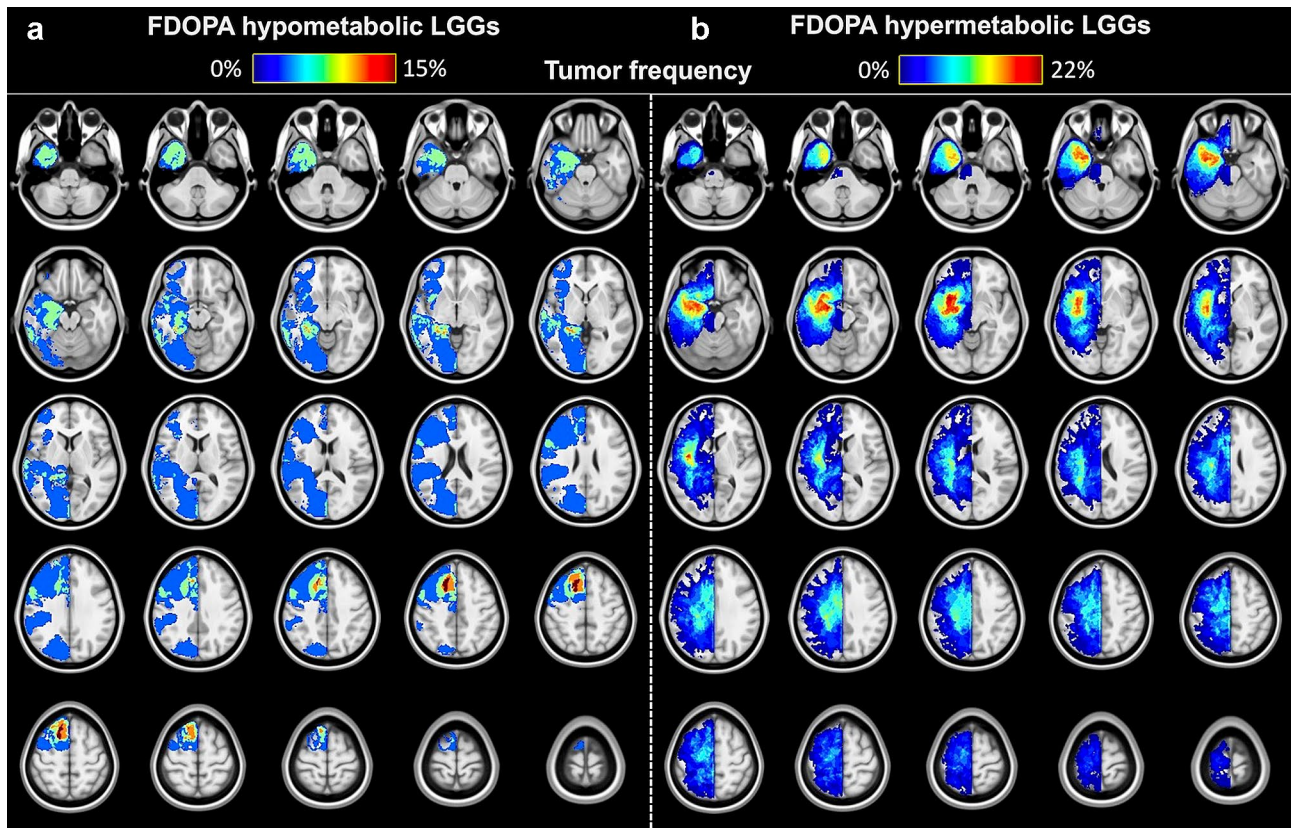
**Fig. 2** Atlas of tumor locations. Voxel-wise frequency of tumor occurrence for FDOPA hypometabolic (n = 14, nSUV$_{max}$ < 1) and hypermetabolic LGGs (n = 37, nSUV$_{max}$ > 1). **a** Frequency of tumor occurrence for FDOPA hypometabolic LGG patients. **b** Frequency of tumor occurrence for FDOPA hypermetabolic LGG patients. Note: All ROIs in the left hemisphere are flipped to the right hemisphere

reported as predominant localizations for LGGs [34, 35]. Cytoarchitectonic and chemoarchitectonic similarities or similar functional roles representing an interface between multimodal areas were suspected to affect the preferential localization in such areas [35]. Our findings are consistent with these previous studies, while revealing more frequent localization in the frontal lobe (close to the SMA) for the FDOPA hypometabolic LGGs and more frequent localization in the insula for the FDOPA hypermetabolic LGGs. As no significant differences were detected in the ratio of tumor grades nor IDH/1p19q molecular status between the different FDOPA metabolic status, other factors are likely to influence the associations of FDOPA uptake and preferential localization for LGGs.

Relatively early detection of the frontal lobe LGGs provides one possible hypothesis to explain preferential frontal lobe localization for FDOPA hypometabolic LGGs. The frontal lobe, especially the SMA, represents a functional interface between the prefrontal cortex and primary sensorimotor areas [35]. Specifically, the SMA plays an important role in the control and coordination of complex motor processes and takes part in programming sequential movement patterns [36]; thus, the frontal lobe LGGs close to

such functionally eloquent areas may easily cause noticeable symptoms. A previous meta-analysis also indicated that LGGs in the frontal lobe were associated with a higher risk of preoperative seizure episodes [5]. Dysfunction of brain regions close to such eloquent areas and seizure episodes may result in early imaging examinations and, subsequently, contribute to early detection of gliomas.

This hypothesis was also supported by our results that patients with FDOPA hypometabolic LGG were significantly younger and represented smaller tumor volume in anatomical images compared to patients with hypermetabolic LGG. Incidentally detected LGGs at a non-symptomatic phase were reported to show younger patient age and smaller tumor volume [37–39]. The duration of the clinically non-symptomatic phase of LGGs was 4–15 years with velocity of diametric expansion at 3.5 mm per year [39, 40]. Meanwhile, gliomas often increased their amino acid tracer uptake throughout the course of the disease [41]. These results suggested that LGGs gradually increased their FDOPA uptake and volume from a non-symptomatic phase, and that FDOPA hypometabolic LGGs were detected at a relatively early phase due to their localization close to the symptomatic regions or by chance. This hypothesis also
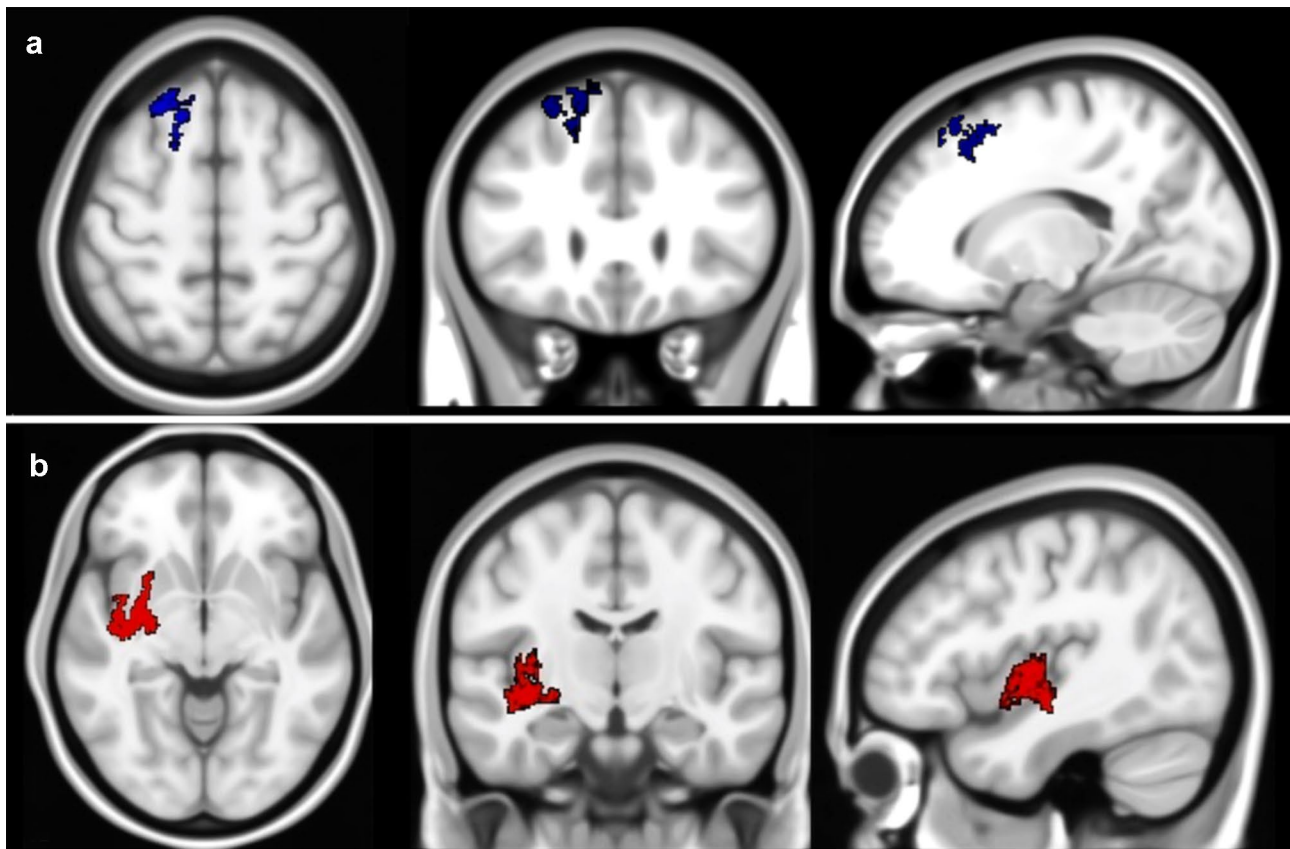
**Fig. 3** ADIFFI statistical analysis isolates two spatially distinct clusters. ADIFFI statistical analysis illustrates **a** a significant cluster occurring in the frontal lobe for FDOPA hypometabolic LGGs ($nSUV_{max} < 1$), and **b** a significant cluster occurring at a high frequency in the insular to putamen for FDOPA hypermetabolic LGGs ($nSUV_{max} > 1$)
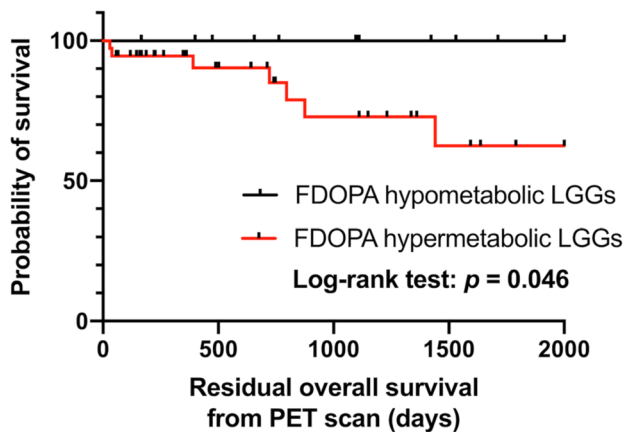


**Fig. 4** The Kaplan–Meier plots and log-rank test show significant differences in overall survival between FDOPA hypometabolic and hypermetabolic LGGs

suggested caution in a case: for example, when a FLAIR hyperintense lesion with FDOPA hypometabolism is identified at the frontal lobe, especially in the eloquent regions, careful follow-up observation or early biopsy, if possible, may be required. Even if it does not show FDOPA hyperuptake, such lesion is perhaps a glioma with an early phase, although FDOPA PET is often used to differentiate primary gliomas from other diseases.

In contrast, the reason why the hypermetabolic LGGs preferentially localized to the insular region was unclear. Epilepsy, cognitive disturbance, and autonomic dysfunction are known symptoms in gliomas involved in the insula [42]. Meanwhile, a homotopic contralateral plasticity due to the slow-growing nature of LGGs may compensate the function of the insula, masking any noticeable symptoms until a relatively late phase [43].

The current study demonstrated that patients with FDOPA hypometabolic LGGs had longer OS than patients with hypermetabolic LGGs, although Cox regression did not show significant association of the OS with the nSUV$_{max}$ or BTV. This was not surprising because amino acid tracer uptake is believed to reflect tumor activities, and several studies have reported better prognosis in patients with lower amino acid tracer uptake gliomas [13, 14]. According to our hypothesis, some hypometabolic gliomas may have been detected at a relatively early phase. On the other hand, some studies have reported a better prognosis in patients with LGGs in the frontal lobe than the other lobes, partly due to the improved rate of complete resection [6, 34, 44, 45]. Thus, the preferential frontal lobe localization and metabolic hypo-activities of LGGs along with a possibility of early detection may interactively contribute to a better prognosis. However, because the prognosis evaluation of this study did not account for the tumor location nor the extent of resection, further validation is needed.

The major limitation of this study was a relatively small population size. Hence, all ROIs in the left hemisphere were flipped to the right hemisphere. It was not possible to evaluate the laterality of LGGs, while asymmetry in human brain structure, function, and gene expression has been documented [46]. Previous studies also described substantial lateralization in specific molecular subtypes of gliomas [9, 10]. A study with a larger population investigating the association of tumor lateralization and amino acid tracer uptake is required. The FDOPA uptake in the normal brain structures may vary in relation to the patient age [47], which may have affected the stratification of gliomas. Other variables, including tumor volume and molecular status, may affect the results of the probability map; however, because of the methodology of the voxel-wised Fisher's exact test, this study could not use these variables as covariates. Instead, this study stratified subjects by a median value of age, FLAIR volume, or BTV, or different molecular status, and compared the frequency of tumor occurrences between subgroups (supplemental data). Other methods such as a general linear model (GLM) may use these parameters as covariates; hence, further validation of the current study is warranted using GLM. Because of retrospective nature the acquisition parameters and scanners of MRI could not be exactly matched across patients, and the Karnofsky performance status were not obtained from all subjects.

## Conclusion

Radiographic atlas analysis revealed that FDOPA hypometabolic LGGs preferentially localized in the frontal lobe. The frontal lobe LGGs in functionally eloquent areas may be detected at a relatively early phase due to symptomatic episodes, which may be associated with tumor hypometabolism, smaller volume, and younger patient age. Understanding such association may lead to improving future management of gliomas.

### Declaration

**Conflicts of interest** Ellingson—Advisory Board—Hoffman La-Roche; Siemens; Nativis; Medicenna; MedQIA; Bristol-Myers Squibb; Imaging Endpoints; Agios. Paid Consultant—Nativis; MedQIA; Siemens; Hoffman La-Roche; Imaging Endpoints; Medicenna; Agios. Grant Funding—Hoffman La-Roche; Siemens; Agios; Janssen. Ellingson also holds a patent on this technology (US Patent #15/577,664; International PCT/US2016/034886). Cloughesy—Advisory Board—Roche/ Genentech, Amgen, Tocagen, NewGen, LPath, Proximagen, Celgene, Vascular Biogenics Ltd, Insys, Agios, Cortice Bioscience, Pfizer, Human Longevity, BMS, Merck, Notable Lab, MedQIA.

**Ethics approval** All procedures performed in studies involving human participants were in accordance with the ethical standards of the institutional and/or national research committee and with the 1964 Helsinki declaration and its later amendments or comparable ethical standards. Written informed consent was obtained from all individual participants to have their imaging, clinical, and molecular data included in our research database (IRB IRB#10-000655).

## References

1. Wang Y, Liu S, Fan X, Li S, Wang R, Wang L, Ma J, Jiang T, Ma W (2015) Age-associated brain regions in gliomas: a volumetric

analysis. J Neurooncol 123:299–306. https://doi.org/10.1007/s11060-015-1798-x

2. Ren X, Cui X, Lin S, Wang J, Jiang Z, Sui D, Li J, Wang Z (2012) Co-deletion of chromosome 1p/19q and IDH1/2 mutation in glioma subsets of brain tumors in Chinese patients. PLoS ONE 7:e32764. https://doi.org/10.1371/journal.pone.0032764

3. Stockhammer F, Misch M, Helms HJ, Lengler U, Prall F, von Deimling A, Hartmann C (2012) IDH1/2 mutations in WHO grade II astrocytomas associated with localization and seizure as the initial symptom. Seizure 21:194–197. https://doi.org/10.1016/j.seizure.2011.12.007

4. Paldor I, Pearce FC, Drummond KJ, Kaye AH (2016) Frontal glioblastoma multiforme may be biologically distinct from non-frontal and multilobar tumors. J Clin Neurosci 34:128–132. https://doi.org/10.1016/j.jocn.2016.05.017

5. Zhang J, Yao L, Peng S, Fang Y, Tang R, Liu J (2019) Correlation between glioma location and preoperative seizures: a systematic review and meta-analysis. Neurosurg Rev 42:603–618. https://doi.org/10.1007/s10143-018-1014-5

6. Smith JS, Chang EF, Lamborn KR, Chang SM, Prados MD, Cha S, Tihan T, Vandenberg S, McDermott MW, Berger MS (2008) Role of extent of resection in the long-term outcome of low-grade hemispheric gliomas. J Clin Oncol 26:1338–1345. https://doi.org/10.1200/JCO.2007.13.9337

7. Bilello M, Akbari H, Da X, Pisapia JM, Mohan S, Wolf RL, O'Rourke DM, Martinez-Lage M, Davatzikos C (2016) Population-based MRI atlases of spatial distribution are specific to patient and tumor characteristics in glioblastoma. Neuroimage Clin 12:34–40. https://doi.org/10.1016/j.nicl.2016.03.007

8. Roux A, Roca P, Edjlali M, Sato K, Zanello M, Dezamis E, Gori P, Lion S, Fleury A, Dhermain F, Meder JF, Chretien F, Lechapt E, Varlet P, Oppenheim C, Pallud J (2019) MRI atlas of IDH wild-type supratentorial glioblastoma: probabilistic maps of phenotype, management, and outcomes. Radiology 293:633–643. https://doi.org/10.1148/radiol.2019190491

9. Ellingson BM, Cloughesy TF, Pope WB, Zaw TM, Phillips H, Lalezari S, Nghiemphu PL, Ibrahim H, Naeini KM, Harris RJ, Lai A (2012) Anatomic localization of O6-methylguanine DNA methyltransferase (MGMT) promoter methylated and unmethylated tumors: a radiographic study in 358 de novo human glioblastomas. Neuroimage 59:908–916. https://doi.org/10.1016/j.neuroimage.2011.09.076

10. Ellingson BM, Lai A, Harris RJ, Selfridge JM, Yong WH, Das K, Pope WB, Nghiemphu PL, Vinters HV, Liau LM, Mischel PS, Cloughesy TF (2013) Probabilistic radiographic atlas of glioblastoma phenotypes. AJNR Am J Neuroradiol 34:533–540. https://doi.org/10.3174/ajnr.A3253

11. Kratochwil C, Combs SE, Leotta K, Afshar-Oromieh A, Rieken S, Debus J, Haberkorn U, Giesel FL (2014) Intra-individual comparison of (1)(8)F-FET and (1)(8)F-DOPA in PET imaging of recurrent brain tumors. Neuro Oncol 16:434–440. https://doi.org/10.1093/neuonc/not199

12. Poulsen SH, Urup T, Grunnet K, Christensen IJ, Larsen VA, Jensen ML, Af Rosenschold PM, Poulsen HS, Law I (2017) The prognostic value of FET PET at radiotherapy planning in newly diagnosed glioblastoma. Eur J Nucl Med Mol Imaging 44:373–381. https://doi.org/10.1007/s00259-016-3494-2

13. Villani V, Carapella CM, Chiaravalloti A, Terrenato I, Piludu F, Vidiri A, Schillaci O, Floris R, Marzi S, Fabi A, Pace A (2015) The role of PET [18F]FDOPA in evaluating low-grade glioma. Anticancer Res 35:5117–5122

14. Patel CB, Fazzari E, Chakhoyan A, Yao J, Raymond C, Nguyen H, Manoukian J, Nguyen N, Pope W, Cloughesy TF, Nghiemphu PL, Czernin J, Lai A, Ellingson BM (2018) (18)F-FDOPA PET and MRI characteristics correlate with degree of malignancy and predict survival in treatment-naive gliomas: a cross-sectional study. J Neurooncol 139:399–409. https://doi.org/10.1007/s11060-018-2877-6

15. Verger A, Metellus P, Sala Q, Colin C, Bialecki E, Taieb D, Chinot O, Figarella-Branger D, Guedj E (2017) IDH mutation is paradoxically associated with higher (18)F-FDOPA PET uptake in diffuse grade II and grade III gliomas. Eur J Nucl Med Mol Imaging 44:1306–1311. https://doi.org/10.1007/s00259-017-3668-6

16. Ginet M, Zaragori T, Marie PY, Roch V, Gauchotte G, Rech F, Blonski M, Lamiral Z, Taillandier L, Imbert L, Verger A (2020) Integration of dynamic parameters in the analysis of (18)F-FDopa PET imaging improves the prediction of molecular features of gliomas. Eur J Nucl Med Mol Imaging 47:1381–1390. https://doi.org/10.1007/s00259-019-04509-y

17. Naslund O, Smits A, Forander P, Laesser M, Bartek J Jr, Gempt J, Liljegren A, Daxberg EL, Jakola AS (2018) Amino acid tracers in PET imaging of diffuse low-grade gliomas: a systematic review of preoperative applications. Acta Neurochir (Wien) 160:1451–1460. https://doi.org/10.1007/s00701-018-3563-3

18. Kertels O, Kessler AF, Mihovilovic MI, Stolzenburg A, Linsenmann T, Samnick S, Brandlein S, Monoranu CM, Ernestus RI, Buck AK, Lohr M, Lapa C (2019) Prognostic value of O-(2-[(18)F]Fluoroethyl)-L-tyrosine PET/CT in newly diagnosed WHO 2016 Grade II and III glioma. Mol Imaging Biol 21:1174–1181. https://doi.org/10.1007/s11307-019-01357-y

19. Isal S, Gauchotte G, Rech F, Blonski M, Planel S, Chawki MB, Karcher G, Marie PY, Taillandier L, Verger A (2018) A high (18)F-FDOPA uptake is associated with a slow growth rate in diffuse Grade II-III gliomas. Br J Radiol 91:20170803. https://doi.org/10.1259/bjr.20170803

20. Cicone F, Carideo L, Scaringi C, Arcella A, Giangaspero F, Scopinaro F, Minniti G (2019) (18)F-DOPA uptake does not correlate with IDH mutation status and 1p/19q co-deletion in glioma. Ann Nucl Med 33:295–302. https://doi.org/10.1007/s12149-018-01328-3

21. Oughourlian TC, Yao J, Schlossman J, Raymond C, Ji M, Tatekawa H, Salamon N, Pope WB, Czernin J, Nghiemphu PL, Lai A, Cloughesy TF, Ellingson BM (2020) Rate of change in maximum (18)F-FDOPA PET uptake and non-enhancing tumor volume predict malignant transformation and overall survival in low-grade gliomas. J Neurooncol 147:135–145. https://doi.org/10.1007/s11060-020-03407-w

22. Tatekawa H, Hagiwara A, Yao J, Oughourlian TC, Ueda I, Uetani H, Raymond C, Lai A, Cloughesy TF, Nghiemphu PL, Liau LM, Pope WB, Salamon N, Ellingson BM (2020) Voxel-wise and patient-wise correlation of 18F-FDOPA PET, rCBV, and ADC in treatment-naïve diffuse gliomas with different molecular subtypes. J Nucl Med 62:319–325

23. Tatekawa H, Hagiwara A, Uetani H, Yao J, Oughourlian TC, Bahri S, Wang C, Raymond C, Lai A, Cloughesy TF, Nghiemphu PL, Liau LM, Pope WB, Salamon N, Ellingson BM (2020) Multiparametric MR-PET measurements in hypermetabolic regions reflect differences in molecular status and tumor grade in treatment-naïve diffuse gliomas. J Neurooncol 149:337–346. https://doi.org/10.1007/s11060-020-03613-6

24. Bishop A, Satyamurthy N, Bida G, Hendry G, Phelps M, Barrio JR (1996) Proton irradiation of [18O]O2: production of [18F]F2 and [18F]F2 + [18F] OF2. Nucl Med Biol 23:189–199. https://doi.org/10.1016/0969-8051(95)02037-3

25. Namavari M, Bishop A, Satyamurthy N, Bida G, Barrio JR (1992) Regioselective radiofluorodestannylation with [18F]F2 and [18F]CH3COOF: a high yield synthesis of 6-[18F]Fluoro-L-dopa. Int J Rad Appl Instrum A 43:989–996. https://doi.org/10.1016/0883-2889(92)90217-3

26. Kinahan PE, Townsend DW, Beyer T, Sashin D (1998) Attenuation correction for a combined 3D PET/CT scanner. Med Phys 25:2046–2053. https://doi.org/10.1118/1.598392

27. Nuyts J, Michel C, Dupont P (2001) Maximum-likelihood expectation-maximization reconstruction of sinograms with arbitrary noise distribution using NEC-transformations. IEEE Trans Med Imaging 20:365–375. https://doi.org/10.1109/42.925290

28. Thie JA (2004) Understanding the standardized uptake value, its methods, and implications for usage. J Nucl Med 45:1431–1434

29. Chen W, Silverman DH, Delaloye S, Czernin J, Kamdar N, Pope W, Satyamurthy N, Schiepers C, Cloughesy T (2006) 18F-FDOPA PET imaging of brain tumors: comparison study with 18F-FDG PET and evaluation of diagnostic accuracy. J Nucl Med 47:904–911

30. Ellingson BM, Kim HJ, Woodworth DC, Pope WB, Cloughesy JN, Harris RJ, Lai A, Nghiemphu PL, Cloughesy TF (2014) Recurrent glioblastoma treated with bevacizumab: contrast-enhanced T1-weighted subtraction maps improve tumor delineation and aid prediction of survival in a multicenter clinical trial. Radiology 271:200–210. https://doi.org/10.1148/radiol.13131305

31. Tran AN, Lai A, Li S, Pope WB, Teixeira S, Harris RJ, Woodworth DC, Nghiemphu PL, Cloughesy TF, Ellingson BM (2014) Increased sensitivity to radiochemotherapy in IDH1 mutant glioblastoma as demonstrated by serial quantitative MR volumetry. Neuro Oncol 16:414–420. https://doi.org/10.1093/neuonc/not198

32. Law I, Albert NL, Arbizu J, Boellaard R, Drzezga A, Galldiks N, la Fougere C, Langen KJ, Lopci E, Lowe V, McConathy J, Quick HH, Sattler B, Schuster DM, Tonn JC, Weller M (2019) Joint EANM/EANO/RANO practice guidelines/SNMMI procedure standards for imaging of gliomas using PET with radiolabelled amino acids and [(18)F]FDG: version 1.0. Eur J Nucl Med Mol Imaging 46:540–557. https://doi.org/10.1007/s00259-018-4207-9

33. Bullmore ET, Suckling J, Overmeyer S, Rabe-Hesketh S, Taylor E, Brammer MJ (1999) Global, voxel, and cluster tests, by theory and permutation, for a difference between two groups of structural MR images of the brain. IEEE Trans Med Imaging 18:32–42. https://doi.org/10.1109/42.750253

34. Parisot S, Darlix A, Baumann C, Zouaoui S, Yordanova Y, Blonski M, Rigau V, Chemouny S, Taillandier L, Bauchet L, Duffau H, Paragios N (2016) A probabilistic atlas of diffuse WHO Grade II glioma locations in the brain. PLoS ONE 11:e0144200. https://doi.org/10.1371/journal.pone.0144200

35. Duffau H, Capelle L (2004) Preferential brain locations of low-grade gliomas. Cancer 100:2622–2626. https://doi.org/10.1002/cncr.20297

36. Krainik A, Lehéricy S, Duffau H, Vlaicu M, Poupon F, Capelle L, Cornu P, Clemenceau S, Sahel M, Valery CA, Boch AL, Mangin JF, Bihan DL, Marsault C (2001) Role of the supplementary motor area in motor deficit following medial frontal lobe surgery. Neurology 57:871–878. https://doi.org/10.1212/wnl.57.5.871

37. Lima GL, Zanello M, Mandonnet E, Taillandier L, Pallud J, Duffau H (2016) Incidental diffuse low-grade gliomas: from early detection to preventive neuro-oncological surgery. Neurosurg Rev 39:377–384. https://doi.org/10.1007/s10143-015-0675-6

38. Potts MB, Smith JS, Molinaro AM, Berger MS (2012) Natural history and surgical management of incidentally discovered low-grade gliomas. J Neurosurg 116:365–372. https://doi.org/10.3171/2011.9.JNS111068

39. Pallud J, Fontaine D, Duffau H, Mandonnet E, Sanai N, Taillandier L, Peruzzi P, Guillevin R, Bauchet L, Bernier V, Baron MH, Guyotat J, Capelle L (2010) Natural history of incidental World Health Organization grade II gliomas. Ann Neurol 68:727–733. https://doi.org/10.1002/ana.22106

40. Pallud J, Capelle L, Taillandier L, Badoual M, Duffau H, Mandonnet E (2013) The silent phase of diffuse low-grade gliomas. Is it when we missed the action? Acta Neurochir (Wien) 155:2237–2242. https://doi.org/10.1007/s00701-013-1886-7

41. Unterrainer M, Schweisthal F, Suchorska B, Wenter V, Schmid-Tannwald C, Fendler WP, Schuller U, Bartenstein P, Tonn JC, Albert NL (2016) Serial 18F-FET PET imaging of primarily 18F-FET-negative glioma: does it make sense? J Nucl Med 57:1177–1182. https://doi.org/10.2967/jnumed.115.171033

42. Mishra A, John AP, Shukla D, Sathyaprabha TN, Devi BI (2018) Autonomic function in insular glioma: an exploratory study. World Neurosurg 118:e951–e955. https://doi.org/10.1016/j.wneu.2018.07.107

43. Almairac F, Duffau H, Herbet G (2018) Contralesional macrostructural plasticity of the insular cortex in patients with glioma: a VBM study. Neurology 91:e1902–e1908. https://doi.org/10.1212/WNL.0000000000006517

44. Capelle L, Fontaine D, Mandonnet E, Taillandier L, Golmard JL, Bauchet L, Pallud J, Peruzzi P, Baron MH, Kujas M, Guyotat J, Guillevin R, Frenay M, Taillibert S, Colin P, Rigau V, Vandenbos F, Pinelli C, Duffau H, French Reseau d'Etude des G (2013) Spontaneous and therapeutic prognostic factors in adult hemispheric World Health Organization Grade II gliomas: a series of 1097 cases: clinical article. J Neurosurg 118:1157–1168. https://doi.org/10.3171/2013.1.JNS121

45. Simpson JR, Horton J, Scott C, Curran WJ, Rubin P, Fischbach J, Isaacson R, Rotman M, Asbell SO, Nelson JS et al (1993) Influence of location and extent of surgical resection on survival of patients with glioblastoma multiforme: results of three consecutive Radiation Therapy Oncology Group (RTOG) clinical trials. Int J Radiat Oncol Biol Phys 26:239–244. https://doi.org/10.1016/0360-3016(93)90203-8

46. Sun T, Patoine C, Abu-Khalil A, Visvader J, Sum E, Cherry TJ, Orkin SH, Geschwind DH, Walsh CA (2005) Early asymmetry of gene transcription in embryonic human left and right cerebral cortex. Science 308:1794–1798. https://doi.org/10.1126/science.1110324

47. Kumakura Y, Vernaleken I, Buchholz HG, Borghammer P, Danielsen E, Gründer G, Heinz A, Bartenstein P, Cumming P (2010) Age-dependent decline of steady state dopamine storage capacity of human brain: an FDOPA PET study. Neurobiol Aging 31:447–463. https://doi.org/10.1016/j.neurobiolaging.2008.05.005

**Publisher's Note** Springer Nature remains neutral with regard to jurisdictional claims in published maps and institutional affiliations.